

Profile evolution of Cr masked features undergoing HBr-inductively coupled plasma etching for use in 25 nm silicon nanoimprint templates

Deirdre L. Olynick^{a)} and J. Alexander Liddle

Lawrence Berkeley National Laboratory, Center for X-ray Optics, 1 Cyclotron Road, MS 2-400, Berkeley, California 94530

Ivo W. Rangelow

Institute of Microstructure and Technologies and Analytics (IMA), University of Kassel, Heinrich Plett Strasse 40, 34132 Germany

(Received 3 June 2005; accepted 8 August 2005; published 16 September 2005)

In nanoimprint template fabrication, the profile of the template features plays a significant role in the profile, release properties, and CD of the imprinted features. We present a study of profile evolution of nanopatterned Si etching for the fabrication of Si nanoimprint templates using a thin Cr hard mask and an HBr inductively coupled plasma (ICP). In this work, we show the effects of chamber pressure, line spacing, mask selectivity, and mask shape on the bowing, notching, microtrenching, and etching rate of nanopatterned silicon for pressures in the range of 2–10 mTorr for line sizes between 20 and 100 nm (1:1 line to space ratio). We observed that, for features with sizes below 50 nm, increasing pressure leads to positively sloped sidewalls and microtrenching. At lower pressures, lower etching rates are observed—together with poorer selectivity and mask faceting. Furthermore, we see a tendency for aspect ratio dependent etching (ARDE) or reactive ion etching (RIE) lag at low pressures. Unlike RIE reactors, dc bias in our ICP etcher decreases with decreasing pressure and constant electrode and ICP power. This suggests that neutral shadowing is the mechanism responsible for ARDE. Under constant power and temperature conditions, due to counterbalancing pressure effects between 2 and 10 mTorr, we obtain optimum imprint profiles at an intermediate pressure of 5 mTorr. © 2005 American Vacuum Society. [DOI: 10.1116/1.2050669]

I. INTRODUCTION

With a theoretical resolution limit in the range of the imprint polymer molecular, nanoimprinting has great potential for nanolithographic applications. However, being a $1\times$ replication process, the high resolution implies that template defects are replicated directly. Thus, reaching the ultimate nanoimprint resolution requires high-resolution high-quality templates. We have developed nanoscale Si templates for single-layer and bilayer nanoimprint lithography used for the production of molecular electronic devices.¹ The Si templates can be used directly for thermoplastic or thermoset imprint resists or transferred to quartz substrates using ultraviolet-curable resists for quartz template replication. An optimally designed template will have feature profiles that resemble a perfect top-hat function. This will allow proper release of the mold while also providing the best mask shape for breakthrough etching and subsequent pattern transfers. Our Si templates are defined by dry etching of single-crystal Si substrates through an electron-beam (e-beam) patterned mask. These Si templates have the advantage of being mechanically robust; however, obtaining top-hat profiles during pattern transfer is difficult. Deviations from the ideal profiles can replicate defects, which are problematic for the imprint process release and breakthrough steps (Fig. 1). Retrograde profiles (sidewall features less than 90° with the horizontal),

which can develop while etching, might be desirable for subsequent lift-off processes but can hinder mold release [Fig. 1(A)]. Other types of etching profiles can exacerbate CD changes during the imprint breakthrough-etching step [Fig. 1(B)]. Precise CD control is very important for small features and has proven even more difficult as patterns become denser.

Profile shape and CD uniformity during etching are determined by a complex set of variables tuned through factors such as inductively coupled plasma (ICP)-power density, reactor pressure, platen power, mask composition (conductivity) and shape. Mechanistic studies of profile development in submicron patterned Si undergoing Cl_2 and HBr dry etching have evolved over the last 10 years.^{2–5} Precise engineering of nanoscale profiles for an imprint necessitates the extension of these studies to the nanoscale regime.

The focus of this work is the development of templates with better than 30 nm resolution and dry etched feature profiles optimized for best imprint results. We pattern dense lithographic features into hydrogen silsesquioxane (HSQ) at feature sizes from 20 to 200 nm employing e-beam lithography (Leica VB6HR tool) and transfer into silicon using an ICP plasma etcher (Oxford Plasma Technology, Ltd). We have studied the effects of etching masks, which have been shown to have a significant influence on the profile development in the submicron regime.^{6,7} Here, we present silicon profile evolution using a Cr hard mask and variable pressure HBr chemistry.

^{a)}Electronic mail: dlolynick@lbl.gov

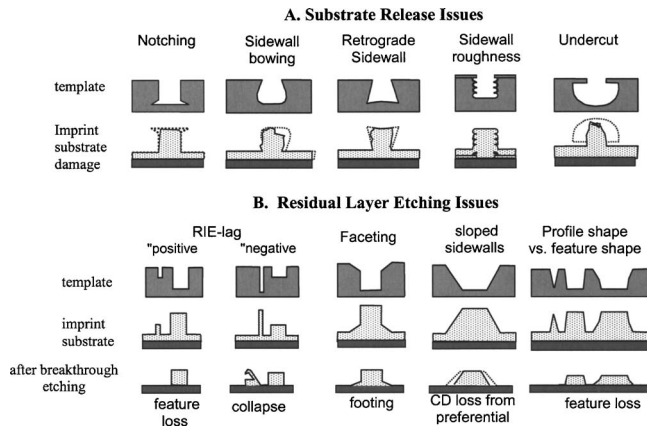


FIG. 1. Effects of template profiles on imprint profiles.

II. EXPERIMENT

A. Hard mask patterning

For the patterning of the hard mask, a three-level process was used. First, a 14 nm Cr layer was formed on 100 mm (100) Si wafers using e-beam evaporation. Next, a barrier layer between the Cr and the imaging layer was created. (This was to forestall any possible Cr/Si interaction as the imaging layer is a silicon-based resist.) Wafers were coated with a 15% weight solution of Sumitomo AZPN114 photoresist spun at 6000 rpm and hard baked at 250 °C for 5 min producing a 35 nm film. Finally, the wafers were coated with the imaging layer: A 1.8% solution of HSQ (Fox-15, Dow Corning, 18% solids) spun at 1000 rpm and oven baked for 5 min on a copper plate at 170 °C producing a 45 nm film.

Patterns were exposed in a modified⁸ Leica VB6HR e-beam lithography tool at 100 keV with a 450 pA beam current and 5 nm spot size. Each sample consisted of lines with pitches 60 to 200 nm and a variable half-pitch.

The HSQ imaging layer was developed in 100% Shipley LDD 26-W for 8 min, rinsed in deionized water and blown dry. All etching was done in a two chamber ICP source Oxford Plasmalab 100 ICP 380 with a shared load lock. Chamber 1 employs fluorine chemistries, oxygen, argon, and nitrogen. Chamber 2 employs chlorine and bromine chemistries, oxygen, argon, and nitrogen. No cross contamination between chambers was observed.

The etching parameters used in our study are shown in Table I. The AZPN114 was dry etched 35 s in Chamber 1 (Recipe 1, Table I) for 35 s. The chromium hard mask was etched in Chamber 2 for 8 min (Recipe 2, Table I). The HSQ/AZPN114 bilayer mask was removed in 100% HF for

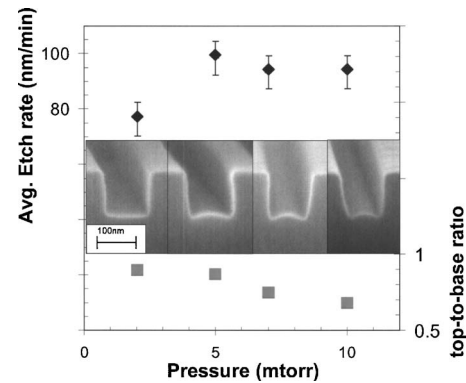


FIG. 2. Pressure effects on 100 nm half-pitch features.

10 s, followed by an oxygen plasma in the Oxford etcher (Recipe 1, Table I, 25C). The samples were then etched using HBr chemistry (Recipe 3, Table I).

III. ETCHING PROFILE DEVELOPMENT

Figure 2 shows the profile development in 100 nm half-pitch lines etched in silicon, at an aspect ratio of 1:1.1 at pressures from 2 to 10 mTorr. The features etched at the lowest pressure are closest to the ideal imprint structure, a top hat with very straight sidewalls, and with only a small amount of mask faceting present. As the pressure is increased, the increased ion angular spread allows a positively sloped profile and microtrenches (small trenches etched deeper than the bulk due to ion focusing) to develop. Graphically, the tradeoff between lower and higher pressures is shown: The 20% decrease in etching rate as pressure is reduced to 2 mTorr is compensated for by the minimization of CD loss. The CD loss at the higher pressures results from the positive sidewall profile while the CD loss at 2 mTorr is a consequence of mask faceting. None of the etching profiles are retrograde, and thus; none would be catastrophic for the imprint process. The etching process window at the 100 nm half-pitch feature size is therefore relatively large and would ultimately be determined by the CD tolerance window.

Figure 3 shows that as the feature half-pitch shrinks, sidewall profiles—albeit similar to the 100 nm half-pitch features—develop defects intolerable for imprint. Here, the etching depth is approximately 115 nm and aspect ratios range from 1:1 to approximately 4:1 at the smallest half-pitch. At 10 mTorr, the positively sloped profiles result in pinched-off features. At 2 mTorr, the defects induced by faceting of the mask become a significant portion of the CD. In addition, at 5 and 7 mTorr, sidewall bowing is apparent

TABLE I. Plasma conditions.

Etching step	Source power (W)	Bias power (W)	Pressure (mTorr)	Chemistry (scm)	Platen temperature (0 °C) (15 Torr He back side)	Etch rate (nm/min)
1. Resist	350	20	1.5	O ₂ 20	-100	100
2. Cr	0	50	90	Cl ₂ 20/O ₂ 2	-20	30
3. Si	700	60	2,5,7,10	HBr 20	20	Var.

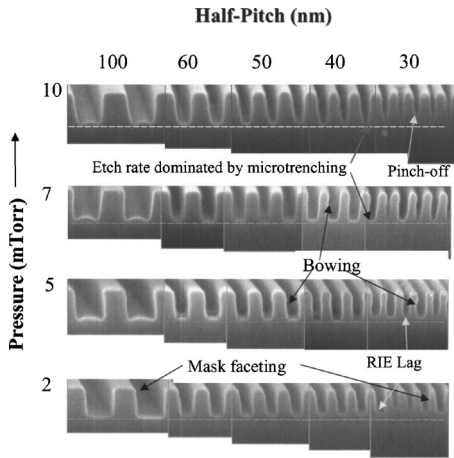


FIG. 3. Effect of pressure and pitch on feature profiles.

and results in a slightly retrograde profile. Although it looks as if the microtrenches apparent in the 100 nm half-pitch features have disappeared, in fact they have merged to form one trench, and are determining the feature etching depths (Fig. 4).

The feature profile evolution—considering effects of microtrenching, sidewall slope, and bowing with pressure and power—has been previously studied and modeled for submicron features etched into silicon with Cl₂, HBr, and Br₂ chemistries.^{2,9–11} These effects are strongly dependent on the angular distribution of ion impacts with the feature sidewall (the angular distribution becomes more forward peaked as the pressure is decreased). Vitale *et al.*¹² measured etching yields in F₂, Cl₂, Br₂, and HBr plasmas in these pressure ranges and showed strong dependencies with the incident ion angle. Near normal incidence, the etching yield is very high but drops off strongly at glancing angle incidence. Ions hitting the sidewall at glancing angles reflect off the sidewall and are focused to the bottom of the feature forming microtrenches [Fig. 5(A)], and at higher pressures (less forward-peaked angular distributions) positively sloped sidewalls. However, if the flux of ions reflected from the sidewall is broadly distributed relative to the feature dimensions, the resulting microtrenches will overlap as the feature dimensions shrink. As the microtrench width approaches one-half

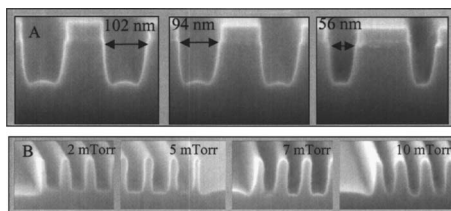


FIG. 4. Etching rate dominated by microtrenching mechanism. (A) As the feature pitch narrows, the microtrenches disappear but the etch depth is the same as the microtrench depth indicating that etching rate is dominated by the glancing angle ions focused to the bottom of the trench. (B) Shows 80 nm pitch lines from 2 to 10 mTorr. At 7 and 10 mTorr, the feature bottom etching rate is the same as the microtrench formed at the edge of the last etched line.

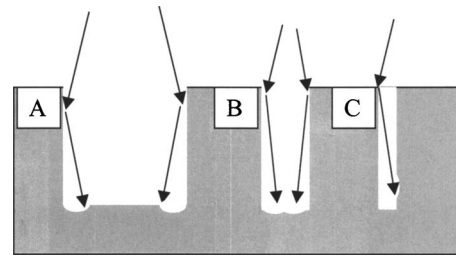


FIG. 5. (A) Glancing angle ions reflected from sidewall form microtrenches. (B) Microtrenches overlap as feature size narrows. (C) Glancing angle ions reflected from sidewall etch opposite sidewall and cause bowing.

of the etched feature, the trenches overlap and dominate the overall etching rate. In our case, the feature sizes are very narrow and the overlap is pronounced [Fig. 5(B)]. Narrowing the feature pitch further allows ions reflected from the feature sidewall to strike the opposite feature sidewall (as opposed to the trench), causing bowing [Fig. 5(C)]. The interesting issue here is that these results show that the ion-sidewall interactions (and thus the ion angular distribution) dominate the profile evolution, even at relatively low aspect ratios (<4:1) and must be understood and controlled for adequate nanoscale pattern transfer.

Figure 6 shows the average etching rate as a function of feature pitch. Reactive ion etching (RIE) lag (a decrease in etching rate with decreasing pitch) is apparent at 2 and 5 mTorr. This is a consequence of aspect ratio dependent etching (ARDE) and has previously been observed for Cl₂ etching of Si in an ICP reactor.¹⁰ ARDE has four possible mechanisms: Knudsen transport, ion shadowing, neutral shadowing, and differential insulator charging.¹³ We believe that we are seeing this lag as a result of neutral shadowing. For ion-assisted etching processes with a perfectly collimated ion stream, the average trench etching rate relative to a plane surface is¹⁴

$$\frac{R_T}{R_P} = \frac{1 + \frac{cF_I}{sF_N}}{1 + \frac{cF_I}{sF_N} \frac{1}{\sqrt{1 + A^2} - A}}, \quad (1)$$

where R_T is the average trench etching rate, R_P is the planar etching rate, c is the ion reaction coefficient, F_I is the ion

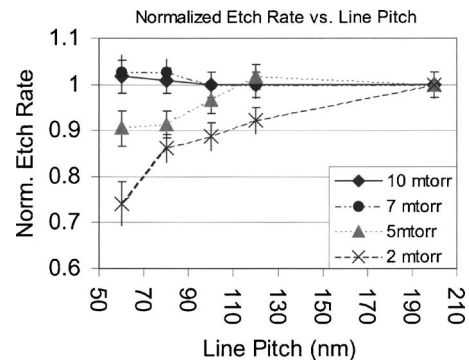


FIG. 6. Etching rate (normalized to largest features) as a function of pitch at 2, 5, 7, and 10 mTorr. RIE lag apparent at 2 and 5 mTorr.

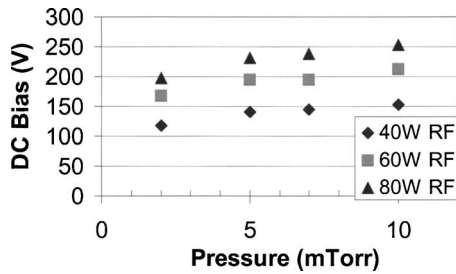


FIG. 7. dc self-bias vs pressure in ICP reactor.

flux, s is the neutral sticking coefficient, F_N is the neutral flux, and A is the trench aspect ratio. Aspect ratio effects become more important as c and/or F_I increase or s and/or F_N decrease.

Contrary to what is often observed in RIE systems, in our ICP system, dc bias decreases with decreasing pressure and constant radio-frequency (rf) power (Fig. 7). Because the rf power is proportional to the ion flux to the substrate times, the dc self-bias, $F_I \propto 1/dc$; the ion flux thus INCREASES as the pressure is reduced. (In an ICP system, better TRANSPORT of the ions from the bulk plasma to the wafer is the most likely reason for this effect. This is a bulk plasma effect—the ions are created close to the ICP coil, and need to be transported to the wafer. Ions do this more efficiently at lower pressures through faster diffusion.)¹⁵ The ion reaction coefficient (ion yield), c , decreases with the square root of dc self-bias. So, the overall effect of decreasing pressure is an increase in the ion (flux) component of etching. Thus, in an ICP system, if we are not sufficiently in excess of neutrals such that $sF_N \gg cF_I$, a pressure reduction will enhance ARDE as is the case with our system. In addition, increasing the ion component of etching decreases selectivity and enhances mask faceting as shown for features etched at 2 mTorr (Fig. 4).

IV. SIMULATIONS

We used a simulator code SPEED (Simulation of Profile Evolution by Etching and Deposition)^{16,17} to better understand the mechanisms leading to the experimentally observed feature profiles. In high-density plasma operating at 2 to 10 mTorr and a typical plasma density of approximately $2 \times 10^{11} \text{ cm}^{-23}$, the sample surface would see an ion flux of approximately 2 to 5 mA/cm² and a neutral flux of approximately 10^{18} neutrals/cm² s. The neutral-to-ion flux ratio would be approximately 50, which corresponds to saturation coverage of neutrals. Consequently, in this pressure regime, it appears that we are ion limited and insensitive to changes in neutral flux (pressure changes). Using this assumption in profile simulation, as well as silicon etching rate as a function of dc bias and ion-impinging angle (etching rate maximum at 5° off-normal impact angle), we have been able to capture the essential characteristics of the experimentally observed profiles at 2 and 7 mTorr (Fig. 8). These profile simulations are done for neutral to ion-flux 45:1, Cr mask thick-

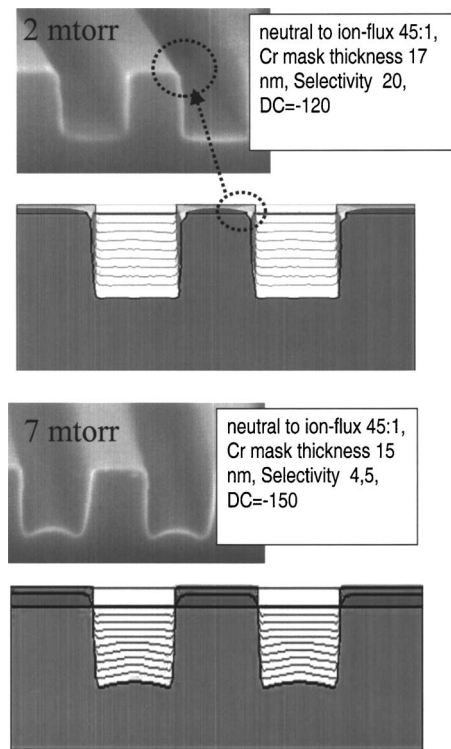


FIG. 8. Simulations of feature profiles at 2 and 7 mTorr.

ness 15–17 nm, Selectivity 5–20, dc=-120 V, etching rate maximum at 5° off-normal impact angle.

These simulations do not obviously explain the magnitude of lag we observed at 2 mTorr (approximately 20% reduction in etch rate from 3:1 aspect ratios). It is difficult to capture all effects in a simulation. Possibly at 2 mTorr, the sputtering of the quartz clamping plate is introducing additional chemistries into the system (i.e., oxygen), which through fast diffusion may be able to play a role in the Si etching. This could impede neutral surface reactions [lower s , Eq. (1)], and increase ARDE effects.

V. CONCLUSIONS

We have studied the effects of pressure and feature size on sub-100 nm features etched into single-crystal silicon with a thin Cr hard mask. Pressure had strong effects on ion angular distributions, which in turn affected feature profiles. Large ion angular distributions at higher pressure produced microtrenches and positive sidewall slope. Narrow ion angular distributions improved sidewall verticality but the required decrease in pressure produced mask edge faceting which can cause a larger CD loss. At 5, 7, and 10 mTorr, as the feature size was reduced, microtrenches merged, and produced trench etch rates faster than that for planar Si etching. Also, bowing was explained as the effect of scattered ions etching the opposite facing feature wall, as opposed to the trench bottoms. At 2 and 5 mTorr, we observed ARDE, which we believe to be due to neutral shadowing of the reacting species. For imprint, the optimum condition was 5 mTorr, as it offered a near top-hat profile without significant lag. Our

simulations using neutral to ion flux ratios between 20 and 100 (i.e., an ion limited regime), were able to capture the essential characteristics of the profile evolution with pressure. Future work will compare nanoscale pattern transfer results with alternative etching masks.

ACKNOWLEDGMENTS

The authors thank M. J. Cooke for valuable insights on ICP ion transport. This work was supported by DARPA MIPR Contract No. 03-8335.

¹Y. Chen *et al.*, *Appl. Phys. Lett.* **82**, 1610 (2003).

²H. H. Hwang *et al.*, *J. Vac. Sci. Technol. B* **20**, 2199 (2002).

³A. P. Mahorowala and H. H. Sawin, *J. Vac. Sci. Technol. B* **20**, 1077 (2002).

⁴M. A. Vyvoda *et al.*, *J. Vac. Sci. Technol. A* **16**, 3247 (1998).

⁵M. A. Vyvoda *et al.*, *J. Vac. Sci. Technol. B* **18**, 820 (2000).

⁶C. Cheng, A. K. V. Guinn, and V. M. Donnelly, *J. Vac. Sci. Technol. B*

14, 85 (1996).

⁷A. P. Mahorowala *et al.*, *J. Vac. Sci. Technol. B* **20**, 1055 (2002).

⁸E. H. Anderson, V. Boegli, and L. P. Muray, *J. Vac. Sci. Technol. B* **13**, 2529 (1993).

⁹M. Li, M. A. Vyvoda, D. B. Graves, H. Lee, M. V. Malyshev, F. P. Klemens, J. T. C. Lee, and V. M. Donnelly, *J. Vac. Sci. Technol. B* **18**, 820 (2000).

¹⁰M. Li, M. A. Vyvoda, and D. B. Graves, *J. Vac. Sci. Technol. A* **17**, 3293 (1999).

¹¹H. Lee, M. A. Vyvoda, M. V. Malyshev, F. P. Klemens, M. Cerullo, V. M. Donnelly, D. B. Graves, A. Kornblit, and J. T. C. Lee, *J. Vac. Sci. Technol. A* **16**, 3247 (1998).

¹²S. A. Vitale, H. Chae, and H. H. Sawin, *J. Vac. Sci. Technol. A* **19**, 2197 (2001).

¹³R. A. Gottscho, C. W. Jurgensen, and D. J. Vitkavage, *J. Vac. Sci. Technol. B* **10**, 2133 (1992).

¹⁴J. M. F. Zachariasse and A. N. Broers, *Microelectron. Eng.* **30**, 349 (1996).

¹⁵M. J. Cooke (personal communication).

¹⁶I. W. Rangelow, P. Thoren, and R. Kassing, *Microelectron. Eng.* **3**, 631 (1985).

¹⁷I. W. Rangelow and A. Fichelscher, *Proc. SPIE* **1392**, 240 (1990).